Applied Surface Science 282 (2013) 17–24

Contents lists available at SciVerse ScienceDirect

Applied Surface Science

journal homepage: www.elsevier.com/locate/apsusc

Benzene adsorption on PtCo(1 1 1): A DFT study

P. Bechthold[a,b], S. Ardenghi[a,b], V. Cardoso Schwindt[a], E.A. González[a,b], P.V. Jasen[a,b], V. Orazi[a], M.E. Pronsato[a,b], A. Juan[a,b,*]

[a] Departamento de Física Universidad Nacional del Sur, Av. Alem 1253, 8000 Bahía Blanca, Argentina
[b] IFISUR (UNS-CONICET), Av. Alem 1253, 8000 Bahía Blanca, Argentina

ARTICLE INFO

Article history:
Received 8 March 2013
Received in revised form 20 April 2013
Accepted 21 April 2013
Available online 23 May 2013

Keywords:
DFT
PtCo
Benzene adsorption
Electronic structure

ABSTRACT

Adsorption benzene on PtCo(1 1 1) surface at low coverage is investigated using density functional theory calculations. We have investigated the PtCo FCT alloy surface with a uniform distribution and two-benzene orientation on the surface. It was found that the most favorable site is a Co—Co bridge with an adsorption energy of −0.37 eV. A large buckling for the first Co and Pt atoms on the surface layers and a 17–30° H-tilt angles are found. The bonding analysis indicates that C—C and C—H bonding increase while Pt—Pt, Co—Co and Pt—Co decrease 13.2, 73 and 33%, respectively, after adsorption benzene. The vibrational frequencies of adsorbed benzene were also calculated.

1. Introduction

The catalytic conversion of aromatic molecules is a very important process in the chemical industry, both for environmental and economical reasons [1,2]. Hydrogenation or hydrogenolysis of these stable hydrocarbon molecules are the main target reactions in petroleum refining and reforming processes which are performed on transition metal catalysts. A strong incentive is provided by the European legislation, which has set a strict limit on the concentration of benzene and other aromatic molecules in fuels [3,4]. As a consequence, the bonding and coordination of aromatic compounds on transition metal surfaces continue to raise a large interest [5].

Benzene is a model compound for aromatic molecules, and although the chemisorption of this molecule has been studied from several experimental [6–9] and theoretical approaches [1,2,5,10], the chemisorption or reactivity properties with respect to it remains an important issue to understand and optimize the catalytic performances.

Even if the basic aspects of benzene adsorption on transition metal surfaces are reasonably well understood, some important aspects, such as the preference for a particular adsorption site, the adsorption energy, or the general mechanism underlying the metal-surface interaction are however more difficult to extract from the experimental approaches, and are still the subject of an active debate [5]. The possibility in some cases of obtaining multiple occupations of adsorption sites makes the picture even more complex. One of the key techniques used to study benzene adsorption is vibrational spectroscopy.

First-principles calculations can bring additional and complementary insights to the problem. They especially provide information or analysis that cannot be easily extracted from experiments such as vibrational frequencies or intensities.

Besides the key electrocatalytic role they serve in fuel cells and glucose sensors, platinum catalysts are important components of automotive catalytic converters, CO gas sensors, petroleum refining, hydrogen production, and anticancer drugs. These applications utilize platinum nanomaterials due to their catalytic ability to oxidize CO and NO_x, dehydrogenate hydrocarbons, and electrolyze water and their ability to inhibit the division of living cells [11]. For example, automotive pollution control systems use catalysts containing Pt, Pd, and Rh to oxidize carbon monoxide and hydrocarbons and reduce oxides of nitrogen.

The Pt—Co alloy system has been used for multiple purposes, because of its interesting magnetic and catalytic behavior [12–15]. On one hand, Pt—Co exhibits a large magnetic anisotropy that can be used for the development of novel data storage media [16]. On the other hand, Pt—Co has been found to be an active catalyst in the Fischer–Tropsch process and low-temperature oxidation and reduction reactions, respectively [9,1]. Nowadays, Pt—Co alloy structures are accessible at different sizes and shapes (nanowires, core–shell structures, nanoparticles, etc.) [17]. But it is

* Corresponding author at: Departamento de Física Universidad Nacional del Sur, Av. Alem 1253, 8000 Bahía Blanca, Argentina. Tel.: +54 0291 4595101x2811; fax: +54 0291 4595142.
E-mail address: cajuan@uns.edu.ar (A. Juan).

0169-4332/$ – see front matter © 2013 Elsevier B.V. All rights reserved.
http://dx.doi.org/10.1016/j.apsusc.2013.04.095

of fundamental importance to examine the relationship between preparation parameters, product structures, and their physiochemical properties. Several preparation parameters, including preparation temperature, are found to be crucial to determine the size and shape of the Pt—Co alloys [16,18–20]. Unfortunately, the structure-properties relationships are still poorly understood from a fundamental point of view. For many bimetallic alloy surfaces, the surface structures are not well-defined because of the disorder of metastable phases which can hardly be mimicked by simple cluster or periodic surface slab models [21].

The effect of Pt—Co bimetallic formation has been studied carefully using EXAFS [22,23]. In these studies, no Pt–Pt coordination was found and Pt atoms mostly interact with Co forming Pt—Co bimetallic bonds.

The observation of enhanced hydrogenation activity over PtCo is consistent with the fact that bimetallic catalysts often show properties that are distinctly different from those of the corresponding monometallic catalysts [24–28]. Many previous investigations combining fundamental surface science studies and theoretical calculations have been performed with the goal of correlating electronic properties of bimetallic surfaces with catalytic properties [27–37].

It is well known that bimetallic catalysts often show properties that are distinctly different from those of the corresponding monometallic catalysts [16–20], including the enhancement of hydrogenation activities. Many investigations combining fundamental surface science studies and theoretical calculations have been performed with the goal of correlating electronic properties of bimetallic surfaces with catalytic properties [24–28,36,38,39].

Lu et al. [40] evaluated from density functional theory (DFT) calculations several silica supported Co-based bimetallic (PtCo, PdCo and RuCo) and the corresponding monometallic catalysts for the low-temperature hydrogenation of benzene. These authors found that the PtCo bimetallic system, possessing the lowest hydrogen binding energy in the subsurface Pt—Co—Pt(1 1 1) structure, showed the highest activity for benzene hydrogenation, which was also in agreement with the trends in the apparent activation barrier and the rate constant for benzene consumption. Both the experimental and theoretical calculation results suggested that PtCo bimetallic catalyst possessed higher activity than other monometallic and bimetallic catalysts.

In a recent work Lu et al. [41] prepared and evaluated the hydrogenation of benzene over PtCo bimetallic and Co, Pt monometallic catalysts supported on γ-Al_2O_3, SiO_2, TiO_2 and activated carbon (AC) at relatively low temperatures (343 K) and atmospheric pressure. According with their results, these authors found that AC supported PtCo bimetallic catalysts exhibited significantly better performance than the other bimetallic catalysts for CO chemisorption capacity and higher hydrogenation activities, and all the bimetallic catalysts possessed higher activity than the corresponding monometallic catalysts. Also these authors provided additional information by extended X-ray absorption fine structure (EXAFS) and transmission electron microscopy (TEM) analysis regarding the formation of Pt—Co bimetallic bonds and metallic particle size distribution in the Pt—Co bimetallic catalysts on different supports.

In this work we modeled the benzene adsorption on a PtCo alloy studying the changes in the electronic structure and chemical bonding after adsorption.

2. The surface model and the computational method

The crystal structure of the Pt—Co alloy presents two-phases. A chemically disordered face centered cubic (FCC) phase, which correspond to low temperature structure, and a chemically ordered $L1_0$ or face-centered tetragonal (FCT) structure for high temperature. In this work we have modeled the last one with a space group P4/mmm. The reason for that choice is that under operation condition in fuels electrodes the high temperature phase is the most stable. Stassi et al. studied the thermal effect on the two stable structure for PtCo alloys and found that both catalysts showed good performance under PEMFC operation; however, the catalyst characterized by the disordered FCC structure performed slightly better at low temperature (80 °C) and full humidification; whereas, the primitive cubic ordered structure catalyst showed superior characteristics both in terms of performance and stability at high temperature (110 °C) and low relative humidity. These last operating conditions are more relevant for automotive applications [42]. The calculated *a* and *c* lattice parameters for Pt—Co FCT bulk are 3.81 and 3.71 Å, respectively. They are in good agreement with the experimental lattice parameters, which are 3.78 and 3.71 Å [43], respectively and also agrees with the values obtained by Hirunsit and Balbuena [44] and other literature values (3.812 and 3.708 Å) [45]. We selected the (1 1 1) crystallographic plane to determinate the benzene adsorption site and its orientation because we found it as the most stable one, in coincidence with previous calculation of Hirunsit and Balbuena [44]. Density Functional Theory (DFT) is used to compute adsorption energies, trace relevant orbital interactions and to discuss the electronic consequences of incorporating C_6H_6 to the surface. In the next sections, we will consider the computational method and the adsorption models.

2.1. Computational method

We performed first principles calculations based on spin polarized DFT. The Vienna Ab-initio Simulation Package (VASP) is used to solve the Kohn-Sham equations with periodic boundary conditions and a plane wave basis set [46–48]. The electron–ion interactions were described by ultra-soft pseudopotentials [49], and the exchange and correlation energies were calculated with the Perdew–Burke–Ernzerhof form of the spin-polarized generalized gradient approximation (GGA-PBE) [50]. We used a kinetic energy cutoff of 300 eV for all calculations, which converges the total energy to ~1 meV/atom and 0.001 Å for the primitive cell of bulk. The Monkhorst–Pack scheme was used for the k-point sampling [51]. Equilibrium lattice constants of 3.81 and 3.71 Å are used with a converged mesh of 7 × 7 × 7. Bader analysis was used to calculate electronic charges of atoms before and after benzene adsorption [52].

We defined the binding energy PtCo—C_6H_6 with respect to isolated atoms as:

$$\Delta E_{ads}(\mathrm{PtCo} + \mathrm{C_6H_6}) = E_{Total}(\mathrm{PtCo} + \mathrm{C_6H_6}) - E_{Total}(\mathrm{PtCo}) - E_{Total}((\mathrm{C_6H_6})_{molec}) \quad (1)$$

where $E_{Total}((C_6H_6)_{molec})$ is the energy of the isolated benzene molecule.

To understand the C_6H_6—PtCo interactions and bonding we used the concept of Density of State (DOS) and the crystal orbital overlap population (COOP) as described by Hoffmann [53]. The COOP curve is a plot of the OP weighted DOS vs energy. Looking at the COOP, we analyze the extent to which specific states contribute to a bond between atoms or orbitals [53]. The Overlap Populations and COOP analysis were performed using the Spanish Initiative for Electronic Simulations with Thousands of Atoms (SIESTA) code [54,55]. We adopted the generalized gradient approximation (GGA) to treat the electronic exchange and correlation effects, as described by Perdew–Burke–Ernzerhof [56]. In all procedures, a split-valence double-ζ basis set of localized numerical atomic orbitals was used, including polarization functions (DZP), with an energy shift of 50 meV and a split norm of 0.15 [55,57]. An energy cutoff of 150 Ry for the grid integration was chosen to represent the

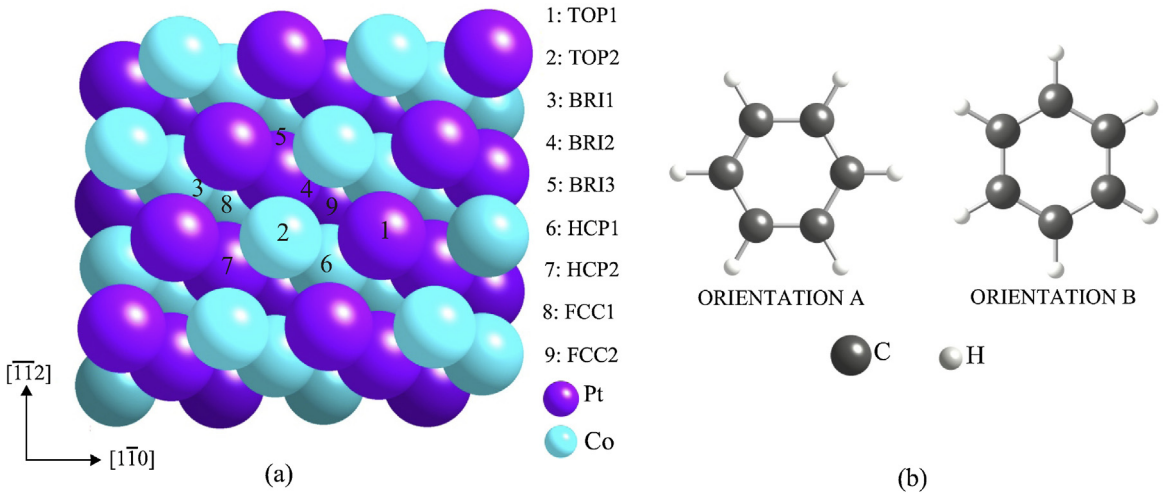

Fig. 1. (a) Schematic top view of PtCo (1 1 1) plane. The high symmetry adsorption sites are indicated. The grading in colors indicates the different and more inner layers. (b) Schematic two possible benzene orientation on the surface. Pt Co.

charge density [54]. The basis set superposition error (BSSE) was eliminated by adding ghost atoms to the calculation on the isolated adsorbate. Ghost atoms possess basis functions as normal but do not otherwise affect the calculation (no projectors, compensation charges, and so on), thereby ensuring that the same degrees of freedom are available to the wave functions in any calculation. This procedure is called the counterpoise method and is described in detail in refs [58]. Standard norm-conserving Troullier–Martins

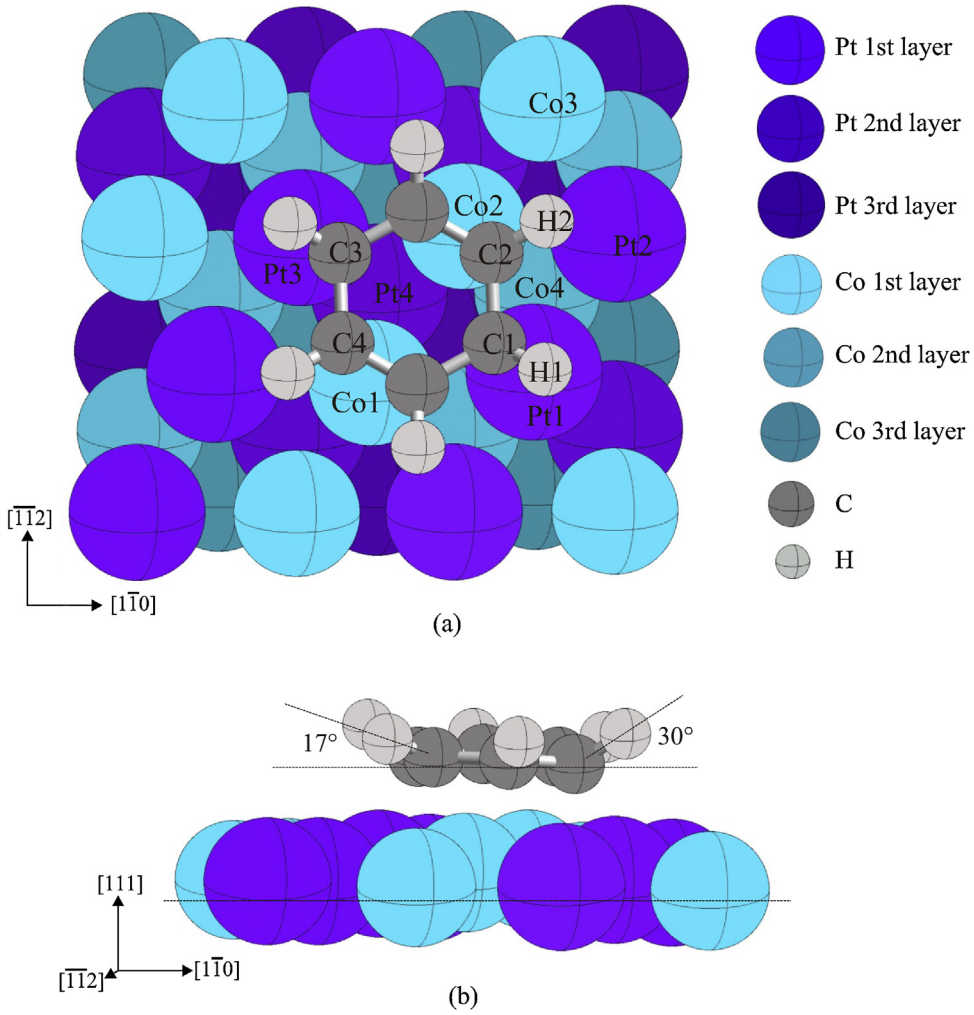

Fig. 2. (a) Schematic top view of the benzene molecule adsorbed in the bridge site (BRI2B) PtCo(1 1 1). The grading in color indicates the inner layers. (b) Schematic lateral view with vertical displacement and C—H angles. Pt Co C H.

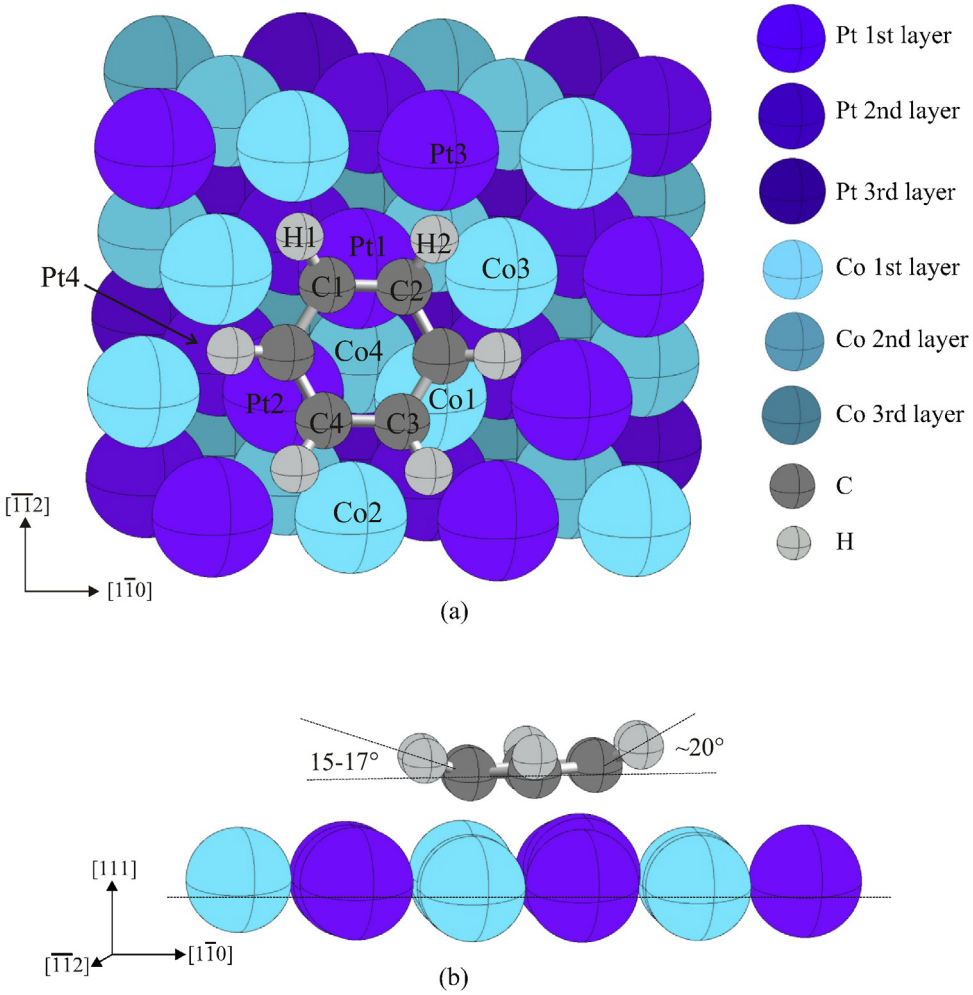

Fig. 3. (a) Schematic top view of the benzene molecule adsorbed in the HCP hollow site (HCP1A) PtCo(1 1 1). The grading in color indicates the inner layers. (b) Schematic lateral view with vertical displacement and C—H angles. Pt Co C H.

pseudopotentials, [59] in their fully separable form [60] were used to describe the electron–ion interaction. The following electronic states were considered as valence in the pseudopotential description of the atoms: Pt:5d9 4 s1; Co 3d7 4s2 C:2s22p2; and H:1s.

2.2. The (1 1 1) surface and the benzene adsorption model

Various ordered atomic planes (0 0 1), (1 0 0), and (1 1 1) in FCT PtCo structure were considered. The most stable plane of PtCo FCT is the (1 1 1). The (1 0 0) and the (1 1 0) planes are −7.2% and −31.4% less stable respectively than the (1 1 1). Therefore, the subsequent calculations on the PtCo FCT system were done only using the FCT PtCo(1 1 1) bulk structure. Note that the results of this study do not address the alloy surface stability, which can be determined using surface free energy and surface segregation energy as recently reported [61].

We represented the (1 1 1) plane with a supercell. In order to achieve the best compromise between computational time and accuracy of our model, we decided to use a six layers slab separated in the [1 1 1]-direction by vacuum regions. The thickness of the vacuum region, corresponding to 6 layers (>13 Å), was enough to avoid interaction of the benzene molecules on the surfaces. The thickness of PtCo(1 1 1) slab should be such that it approaches the electronic structure of 3D bulk PtCo in its innermost layer. Our slab has two surface-like layers and four inner layers. For the sake of clarity Fig. 1a only shows the first three layers of the slab.

For benzene adsorption on the PtCo(1 1 1) surface at low coverage, the molecule-surface distance was optimized considering relaxation for the first four layers of the metal slab until 1 meV convergence is obtained in the total energy; the three remaining layers (bulk like) were maintained (kept) fixed. We mapped the molecular adsorption in all the high symmetry sites and for two different benzene orientations (A and B) (see Fig. 1b). The different adsorption sites have more than one chemical environment and we considered the adsorption on all of them (see Fig. 1a). These sites are top (TOP1: Pt atom, TOP2: Co atom), bridge (BRI1: Pt—Pt atoms, BRI2: Co—Co atoms, BRI3: Pt—Co atoms), FCC (FCC1: Pt—Pt—Co atoms, FCC2: Pt—Co—Co atoms) and HCP (HCP1: Pt—Pt—Co atoms, HCP2: Pt—Co—Co atoms).

3. Results and discussion

Let us first present some results for the clean $Pt_{50}Co_{50}$ (1 1 1) alloy surface. In a recent research, Hirunsit and Balbuena [44] analyzed the problems in alloy catalysis regarding the assessment of surface composition. As mentioned before, for a given bulk composition, different atomic distribution on the surface (and subsurface) are possible.

The computed Pt and Co electron orbital populations are $6s^{1.06}$ $6p^{1.94}$ $5d^{8.80}$ and $4s^{0.47}$ $4p^{0.20}$ $3d^{6.07}$ respectively. A charge transfer is computed from Co to Pt as expected from the electronegativity difference. The width of the d band is about 7.5 eV. The electronic

Table 1
Electron density, overlap population, charge and distances for PtCo(1 1 1) clean and C_6H_6 slab (vacuum). (surf = surface; sub = subsurface).

Structure	Electronic occupation			Bond type	OP	Distances (Å)
	s	p	d			
PtCo(1 1 1)						
Pt_{surf}	1.06	1.94	8.80	Pt_{surf}—Pt_{surf}	0.663	2.650
Pt_{surf}	1.06	1.93	8.79			
Pt_{sub}	0.95	1.73	8.25	Pt_{surf}—Pt_{sub}	0.471	2.715
Co_{surf}	0.47	0.20	6.07	Co_{surf}—Co_{surf}	0.128	2.664
Co_{surf}	0.47	0.21	6.12			
Co_{sub}	0.41	0.16	5.48	Co_{surf}—Co_{sub}	0.108	2.631
				Pt_{surf}—Co_{surf}	0.237	2.673
				Pt_{surf}—Co_{surf}	0.219	2.618
C_6H_6 slab						
C	0.93	1.46	0.00	C—C	0.740	1.398
H	0.89	0.00	0.00	H—H	0.000	2.490
				C—H	0.754	1.092

structure of the surface atoms analyzed through the total and local DOS (see Figs. 4a and 5a, b) shows a similar behavior than that reported by Hirunsit and Balbuena for FCT PtCo structure [44].

The OP between two Pt atoms on the surface is higher than that nn Pt_{surf}–Pt_{sub} (surf = atom from the surface, sub = atom from the subsurface), which is expected because the distance on the surface after optimization is shorter. In the case of Co—Co bonding, the OP are similar and also the sup–sup, sup–sub distances. Table 1 and the COOP plots show intermetallic Pt—Co bonds with an average OP of 0.228. Figs. 6a–c and 7a–c indicate that metal–metal interactions are almost bonding with a little antibonding contribution very near E_F.

From all considered benzene adsorption sites (see Fig. 1), the most favorable results to be the BRI2 Co—Co surface sites with the ring in B orientation (see Fig. 2) with an energy of −0.37 eV. Pussi et al. [62] reported an adsorption energy of −0.25 eV for benzene in pure Co(0 0 0 1) while Morin et al. [63] reported values from −0.26 eV to −1.27 eV in pure Pt FCC. The other site in Pt—Co (HCP1) is less stable (-0.28 eV) with benzene in A orientation. The optimized geometry from DFT calculation is shown in Figs. 3 and 4 and the distances in Tables 2 and 3. The site BRI 1 A is an instable possible adsorption site with energy of −0.18 eV meanwhile the rest sites are not favorable for the adsorption. The benzene ring geometry is slightly distorted in both adsorption sites. Barzen et al. [64] also reported a tilt of the benzene plane with respect to the metal cluster (Co_nPt_m, $n+m \leq 3$). Morin et al. [63] reported that all C atoms in the ring are equivalent with an average ring radio of 1.445 Å with a small Kekulé distortion when adsorbed on Pt(1 1 1). The carbon atoms of the benzene molecule lie ∼2.10 Å above the first surface layer and the carbon ring is slightly expanded —C—C increase from 1.398 Å in vacuum to 1.431 and 1.475 Å- in HCP1 and BRI2 respectively). Similar behavior is reported by Morin et al. [63]. In both sites (BRI2 and HCP1) the metal atoms below the benzene

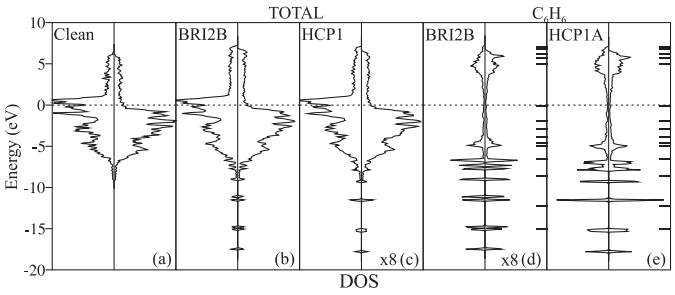

Fig. 4. Total DOS curves for (a) clean surface, (b) after benzene adsorption in BRI2B and (c) after benzene adsorption in HCP1A. DOS curves for the benzene molecule after adsorption in (d) bridge site and (e) hollow site.

moves upward to the C-ring. Large buckling was found for the first Co or Pt atoms on the surface layer around -0.06 – 0.20 Å. Similar buckling in the first substrate layer was also reported by Pussi et al. [62], Morin et al. [63], Mittendorfer and Hafner [65], and Yamagishi et al. [66]. The shortest C—Co bond was found to be 2.132 Å (HCP1) and 2.145 Å (BRI2). This value is smaller than that of Pussi et al. [62] reported from LEED measurements (2.26 ± 0.09 Å). In the case of Pt FCC, Wander et al. [67] reported a C—Pt distance of 2.25 ± 0.05 Å, which is comparable with our computed values of 2.237 (HCP1) and 2.173 (BRI2). Morin et al. [63] computed a C—Pt, for Pt FCC, distance of 2.20 Å. Our computed H-tilt angles in the bridge site are 17° on a Pt center and 30° on a Co center. In the HCP site, the values are ∼20° and 16° on the same centers respectively. Morin et al. [63] computed a H-tilt angles of 37.2° and 15.5° for different C—H bonds in Pt and González et al. [68] reported an H-ring angle of 12° in pure Co HCP.

The electronic structure (DOS plots) in Figs. 4b, e and 5c, f shows a series of small peaks below −9.2 eV coming from benzene molecular orbitals stabilized after adsorption (see the bars on the right in Fig. 4d and e). A higher hybridization in the region (−6.5, −9.2) eV is present in the BRI2B site showing an interaction of benzene orbitals with the bottom of the d metal band (see Fig. 5c and d).

Regarding the bonding, the picture is different in the HCP and BRI sites. In the HCP sites almost all metal—metal bonds OP decrease, being the most affected the intermetallic bond (see Table 3 and COOP curves in Fig. 7) while Pt—C and Co—C bonds are developed (Pt1-C, Co1-C3 in Fig. 3).

The C—C OP in both sites increase due to bonding interaction with the d metal bond (see bands between -6.9 eV to -1.5 eV) (compare Fig. 8a, vacuum, with b and c). Similar behavior is detected for the C—H bonds (compare Fig. 8d with e and f). In the case of the bridge adsorption site, the Pt—Pt bond OP decrease 13.2% (see Fig. 6a), the Co1—Co2 bond OP decrease about 73%, which is expected because they are the atoms that form the bridge. The displacement of these bridge atoms decreases the metal–metal distance (from 2.664 to 2.486 Å) between two neighboring Co atoms,

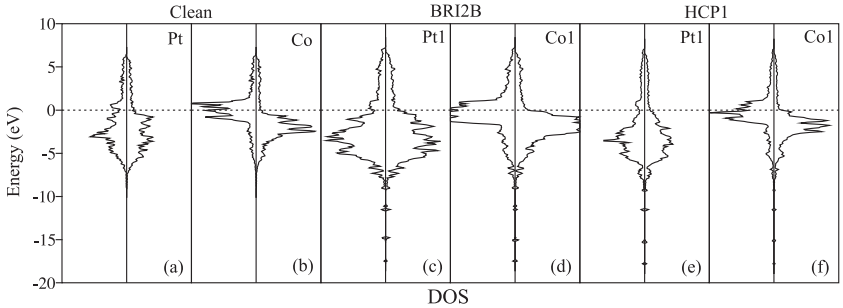

Fig. 5. Projected DOS curves for Pt atoms and Co atoms at clean surface (a) and (b); after benzene adsorption in BRI2B site (c) and (d), and after benzene adsorption in HCP1A site (e) and (f).

Table 2
Electron density, overlap population, ΔOP%, Δcharge and distances for $(C_6H_6)_{BRI2B}$/PtCo(1 1 1).

Structure	Electronic occupation			ΔCharge	Bond type[a]	OP	ΔOP%[b]	Distances (Å)
	s	p	d					
Pt1	0.91	1.71	8.51	0.665	Pt1—Pt2	0.576	−13.2	2.676
Pt2	1.03	1.79	8.69	0.269				
Co1	0.34	0.17	6.16	0.075	Co1—Co2	0.034	−73.4	3.010
Co2	0.33	0.17	5.29	0.240				
					Pt1—Co1	0.158	−33.5	2.692
C1	0.95	3.11	0.00	−1.959	C1—C2	0.925	+25.0	1.475
H1	1.02	0.00	0.00	−0.245	H1—H2	0.000	0.0	2.468
					C1—H1	0.884	+17.2	1.099
					Pt1—C1	0.483	–	2.186
C4	0.96	3.10	0.00	−1.977	Co1—C4	0.175	–	2.126

[a] The geometry of the OP is shown in Fig. 2a.
[b] The percentage of chance is respect to the clean surface or the molecule in vacuum.

Table 3
Electron density, overlap population, ΔOP%, charge and distances for $(C_6H_6)_{HCP1A}$/PtCo(1 1 1).

Structure	Electronic occupation			ΔCharge	Bond type[a]	OP	ΔOP%[b]	Distances (Å)
	s	p	d					
Pt1	0.85	1.62	8.38	0.932	Pt1—Pt2	0.483	−27.1	2.710
Pt2	0.85	1.65	8.37	0.918				
Co1	0.33	0.18	6.31	0.017	Co1—Co2	0.101	−21.1	2.685
Co2	0.43	0.17	5.93	0.228				
					Pt1—Co1	0.179	−24.5	2.745
C1	0.94	3.01	0.00	−1.867	C1—C2	0.925	25.0	1.457
H1	1.03	0.00	0.00	−0.253	H1—H2	0.000	0.0	2.497
					C1—H1	0.892	18.6	1.094
C3	0.96	3.13	0.00	−2.008	Co1—C3	0.181		2.132
					Pt1—C1	0.346		2.237

[a] The geometry of the OP is shown in Fig. 3a.
[b] The percentage of chance is respect to the clean surface or the molecule in vacuum.

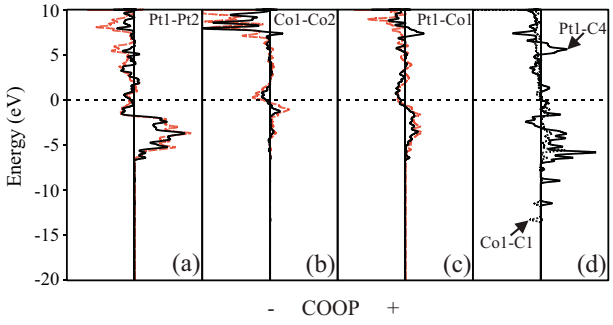

Fig. 6. COOP curves for (a) Pt—Pt, (b) Co—Co, (c) Pt—Co and (d) Co—C and Pt—C bonds for clean surface (red dashed line) and after benzene adsorption in the BRI 2B site (black fill line). (For interpretation of the references to color in this figure legend, the reader is referred to the web version of the article.)

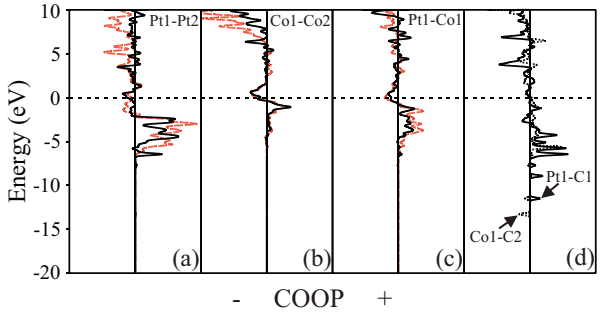

Fig. 7. COOP curves for (a) Pt—Pt, (b) Co—Co, (c) Pt—Co and (d) Co—C and Pt—C bonds for clean surface (red dashed line) and after benzene adsorption in the HCP 1A site (black fill line). (For interpretation of the references to color in this figure legend, the reader is referred to the web version of the article.)

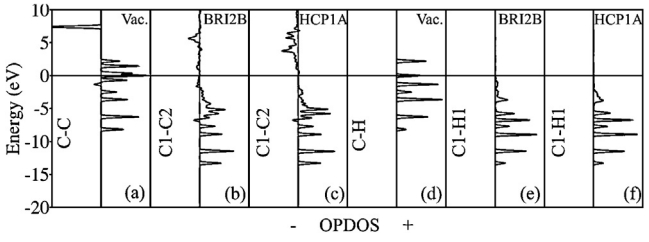

Fig. 8. COOP curves for C—C and C—H bonds for benzene in vacuum (a) and (d), after adsorption on BRI 2B site (b) and (e) and after adsorption in HCP 1A site (c) and (f).

which overlap population increases (49%). Again, the Pt—Co intermetallic bond decreases about 33%. A Pt—C and Co—C bonds are also developed (see Fig. 6).

Finally, we also computed the vibrational frequencies for the chemisorbed molecule. As a reference, the vibrational frequencies of gas-phase benzene were first calculated for the A_{1g} and B_{2u} modes [69]. The obtained values and the experimental ones are listed in Table 4 [69–71]. The agreement is very good with a maximum difference of ∼4%. The vibrational frequencies calculated for

Table 4
Frequencies of the A_{1g} and B_{2u} modes of benzene (in cm^{-1}).

	Exp.[a]	PW91[b]	Gaussian[b,c]	This work
A_{1g}	993	992	1001, 1013	1014
A_{1g}	3074	3129	3149, 3201	3205
B_{2u}	1150	1136	1156, 1164	1143
B_{2u}	1309	1352	1366, 1351	1360

[a] Taken from Ref. [70].
[b] Taken from Ref. [69].
[c] Taken from Ref. [71].

Table 5
Frequencies of the A_{1g} and B_{2u} modes of benzene adsorbed (in cm^{-1}).

	Pt(1 1 1)[a]		Pt(1 1 1)[b]	This work	
	BRI 30°	HCP 0°	HREELS	BRI 2B	HCP 1A
A_{1g}	826	860	825	835	870
A_{1g}	3103	3125	3015	3022	3050
B_{2u}	1140	1154	1130	1136	1139
B_{2u}	1313	1345	1305	1321	1333

[a] Taken from Ref. [57].
[b] Taken from Ref. [72].

the adsorbed molecule are listed in Table 5 for the two sites that were previously considered. The frequencies differ from those in the gas-phase being red-shifted and are similar to those in pure FCC Pt(1 1 1) [72]. The lowering in the vibration frequencies modes involving C—C bonds is consistent with the stretching of these bonds (see Tables 1–3) and Pt, Co—C bond formation. Lehwald et al. have explained the shifts in HREELS vibration frequencies of benzene on Pt (1 1 1) and Ni(1 1 1) by electronic interaction between the metal d-orbitals and molecules adsorbed in on top and three-fold hollow sites respectively [73]. A detailed study of vibration spectra of benzene molecule adsorbed in Pt(1 1 1) was reported by Morin et al. [63].

4. Conclusions

We investigated the benzene adsorption on PtCo FCT alloy with an uniform distribution of metallic atoms. The most favorable site is a bridge Co—Co. The adsorption energy is −0.37 eV and lies between values for pure Co HCP and Pt FCC. A large buckling is computed for both Pt and Co surface atoms. Asymmetrical H-tilt angles for benzene is detected being 17° one Pt center and 30° on a Co center. A higher hybridization is found in the bridge Co site showing the interaction of benzene orbitals with the bottom of the d metal band. The C—C and C—H bonding increase with the Pt—Pt, Co—Co and Pt—Co bonding decrease 13.2, 73 and 33% respectively after adsorption. The calculated vibrational frequencies for adsorbed benzene are similar to those reported for Pt(1 1 1) with a red-shift compared to gas-phase.

Acknowledgements

Our work was supported by ANPCyT through PICT 1770, and PIP-CONICET Nos. 114-200901-00272 and 114-200901-00068 research grants, as well as by SGCyT-UNS. A.J., M.E.P, E.A.G. and P.V.J. are members of CONICET. P.B. and S.A. are fellow researchers at this institution. V.O. is a fellow of Comision Investigaciones Cientificas (CIC-BA).

References

[1] M. Sayes, M.-F. Reyniers, G.B. Marin, M. Neurock, Journal of Physical Chemistry B 106 (2002) 7489.
[2] M. Sayes, M.-F. Reyniers, M. Neurock, G.B. Marin, Journal of Physical Chemistry B 107 (2003) 3844.
[3] B.H. Cooper, B.B.L. Donnis, Applied Catalysis A: General 137 (1996) 203.
[4] A. Stanislaus, B.H. Cooper, Catalysis Reviews: Science and Engineering 36 (1994) 75.
[5] C. Morin, D. Simon, P. Sautet, Journal of Physical Chemistry B108 (2004) 5653.
[6] P. Gomez-Romero, Advanced Materials 13 (2001) 163.
[7] F.S. Tautz, Progress in Surface Science 82 (2007) 479.
[8] H. Ihm, H.M. Ajo, J.M. Gottfried, P. Bera, C.T. Campbell, Journal of Physical Chemistry B 108 (2004) 14627.
[9] S.J. Jenkins, Proceedings of the Royal Society A 465 (2009) 2949.
[10] F. Mittendorfer, C. Thomazeau, P. Raybaud, H. Toulhoat, Journal of Physical Chemistry B 107 (2003) 12287.
[11] A. Cheng, P. Holt-Hindle, Chemical Reviews 110 (2010) 3767.
[12] J.L. Park, M.G. Kim, Y.W. Jun, J.S. Lee, W.R. Lee, J. Cheon, Journal of the American Chemical Society 126 (2004) 9072.
[13] Z.T. Zhang, D.A. Blom, Z. Gai, J.R. Thompson, J. Shen, S. Dai, Journal of the American Chemical Society 125 (2003) 7528.
[14] Y.D. Qian, W. Wen, P.A. Adcock, Z. Jiang, N. Hakim, M.S. Saha, S. Mukerjee, Journal of Physical Chemistry C 112 (2008) 1146.
[15] J.C. Sotelo, J.M. Seminario, Journal of Chemical Physics 127 (2007) 244706.
[16] M. De Santis, R. Baudoing-Savois, P. Dolle, M.C. Saint-Lager, Physical Review B 66 (2002) 085412.
[17] J. Penuelas, P. Andreazza, C. Andreazza-Vignolle, H.C.N. Tolentino, M. De Santis, C. Mottet, Physical Review Letters 100 (2008) 115502.
[18] J.S. Tsay, C.S. Shern, Surface Science 396 (1998) 313.
[19] R. Baudoing-Savois, P. Dolle, Y. Gauthier, M.C. Saint-Lager, M. De Santis, V. Jahns, Journal of Physics: Condensed Matter 11 (1999) 8355.
[20] M.C. Saint-Lager, R. Baudoing-Savois, M. De Santis, P. Dolle, Y. Gauthier, Surface Science 418 (1998) 485.
[21] W.-L. Yim, T. Klüner, Journal of Physical Chemistry C 114 (2010) 7141.
[22] G. Jacobs, J.A. Chaney, P.M. Patterson, T.K. Das, J.C. Maillot, B.H. Davis, Journal of Synchrotron Radiation 11 (2004) 414.
[23] L. Guczi, D. Bazin, I. Kovacs, L. Borko, Z. Schay, J. Lynch, P. Parent, C. Lafon, G. Stefler, Z. Koppany, I. Sajo, Topics in Catalysis 20 (2002) 129.
[24] J.H. Sinfelt, Accounts of Chemical Research 10 (1977) 15.
[25] J.H. Sinfelt, Bimetallic Catalysts: Discoveries, Concepts, and Applications, John Wiley & Sons, New York, 1983.
[26] J.A. Rodriguez, Surface Science Reports 24 (1996) 225.
[27] B. Hammer, J.K. Nørskov, Surface Science 343 (1995) 211.
[28] D.W. Goodman, Journal of Physical Chemistry 100 (1996) 13090.
[29] V. Pallassana, M. Neurock, Journal of Catalysis 191 (2000) 301.
[30] J.G. Chen, C.A. Menning, M.B. Zellner, Surface Science Reports 63 (2008) 201.
[31] J. Greeley, M. Mavrikakis, Nature Materials 3 (2004) 810.
[32] H.H. Hwu, J. Eng Jr., J.G. Chen, Journal of the American Chemical Society 124 (2002) 702.
[33] N.A. Khan, L.E. Murillo, J.G. Chen, Journal of Physical Chemistry B 108 (2004) 15748.
[34] J.R. Kitchin, J.K. Nørskov, M.A. Barteau, J.G. Chen, Physical Review Letters 93 (2004) 156801.
[35] C.A. Menning, H.H. Hwu, J.G. Chen, Journal of Physical Chemistry 110 (2006) 15471.
[36] L.E. Murillo, A.M. Goda, J.G. Chen, Journal of the American Chemical Society 129 (2007) 7101.
[37] M.P. Humbert, J.G. Chen, Journal of Catalysis 257 (2008) 297.
[38] J.R. Kitchin, N.A. Khan, M.A. Barteau, J.G. Chen, B. Yakshinksiy, T.E. Madey, Surface Science 544 (2003) 295.
[39] M.P. Humbert, L.E. Murillo, J.G. Chen, ChemPhysChem 9 (2008) 1262.
[40] S. Lu, C.A. Menning, Y. Zhu, J.G. Chen, ChemPhysChem 10 (2009) 1763.
[41] S. Lu, W.W. Lonergan, Y. Zhu, Y. Xie, J. Chen, Applied Catalysis B: Environmental 91 (2009) 610.
[42] A. Stassi, I. Gatto, G. Monforte, V. Baglio, E. Passalacqua, V. Antonucci, A.S. Aricò, Journal of Power Sources 208 (2012) 35.
[43] L. Xiong, A. Manthiram, Journal of Electrochemical Society 152 (2005) A697.
[44] P. Hirunsit, P.B. Balbuena, Surface Science 603 (2009) 912.
[45] W.B. Pearson, A Handbook of Lattice Spacings and Structures of Metals and Alloys, Pergamon, Oxford, 1964, pp. 1958–1967.
[46] G. Kresse, J. Hafner, Physical Review B 47 (1993) 558.
[47] G. Kresse, J. Furthmüller, Physical Review B 54 (1996) 1 1 169.
[48] G. Kresse, J. Furthmüller, Computation Materials Science 6 (1996) 15.
[49] D. Vanderbilt, Physical Review B 41 (1990) 7892.
[50] J. Perdew, J.A. Chevary, S.H. Vosko, K.A. Jackson, M.R. Pederson, D.J. Singh, C. Fiolhais, Physical Review B 46 (1992) 6671.
[51] H.J. Monkhorst, J.D. Pack, Physical Review B 13 (1976) 5188.
[52] R.F.W. Bader, Atoms in Molecules: A Quantum Theory, Oxford University Press, Oxford, 1990.
[53] R. Hoffmann, Solid & Surface: A Chemist's View of Bonding in Extended Structures, 1st ed., VCH, New York, 1989.
[54] P. Ordejón, E. Artacho, J.M. Soler, Physical Review B 53 (1996) R10441.
[55] J.M. Soler, E. Artacho, J.D. Gale, A. Garcia, J. Junquera, P. Ordejón, D. Sanchez-Portal, Journal of Physics: Condensed Matter 14 (2002) 2745.
[56] J.P. Perdew, K. Burke, M. Ernzerhof, Physical Review Letters 77 (1996) 3865.
[57] J. Junquera, O. Paz, D. Sanchez-Portal, E. Artacho, Physical Review B 64 (2001) 235111.
[58] S.B. Boys, F. Bernardi, Molecular Physics 19 (1970) 553.
[59] N. Troullier, J.L. Martins, Physical Review B 43 (1991) 1993.
[60] L. Kleinman, D.M. Bylander, Physical Review Letters 48 (1982) 1425.
[61] R.K. John, R. Karsten, S. Matthias, Physical Review B 77 (2008) 075437.
[62] K. Pussi, M. Lindroos, J. Katainen, K. Habermehl-Cwirzen, J. Lahtinen, A.P. Seitsonen, Surface Science 572 (2004) 1.
[63] C. Morin, D. Simon, P. Sautet, Journal of Physical Chemistry B 107 (2003) 2995.
[64] L. Barzen, M. Tombers, C. Merkert, J. Hewer, G. Niedner-Schatterburg, International Journal of Mass Spectrometry 330–332 (2012) 271.
[65] F. Mittendorfer, J. Hafner, Surface Science 472 (2001) 133.
[66] S. Yamagishi, S.J. Jenkins, D.A. King, Journal of Chemical Physics 114 (2001) 5765.

[67] A. Wander, G. Held, R.Q. Hwang, G.S. Blackman, M.L. Xu, P. de Andres, M.A. Van Hove, G.A. Somorjai, Surface Science 249 (1991) 21.
[68] E.A. González, P.V. Jasen, J. Pierini, A. Juan, G. Brizuela, Surface Review and Letters 16 (5) (2009) 749.
[69] G. Sun, J. Kürti, P. Rajczy, M. Kertesz, J. Hafner, G. Kresse, Journal of Molecular Structure: THEOCHEM 624 (2003) 37.
[70] L. Goodman, A.G. Ozkabak, S.N. Thakur, Journal of Physical Chemistry 95 (1991) 9044.
[71] A.M. Gardner, T.G. Wright, Journal of Chemical Physics 135 (2011) 114305.
[72] V. Demers-Carpentier, P.H. McBreen, Journal of Physical Chemistry C 115 (2011) 6513.
[73] S. Lehwald, H. Ibach, J.E. Demuth, Surface Science 78 (3) (1978) 577.